END-TO-END IMRT EVALUATION USING SEMI-ANTHROPOMORPHIC THORAX PHANTOM

ANDREEA A. UDREA[1,2*], MIHAI T. DUMITRACHE[1], ALINA DUMITRACHE[1], MARIA VLĂSCEANU[1], AUREL I. POPESCU[2]

[1]*Emergency Central Military Hospital "Dr. Carol Davila", Bucharest, Romania*
[2]*University of Bucharest, Faculty of Physics, Măgurele, Romania*

[*]Corresponding author: *andreeaaudrea@gmail.com*

Abstract. The purpose of this study was to evaluate the intensity modulated radiation therapy (IMRT) workflow using the "end-to-end" approach, i.e. following, with the aid of a semi-anthropomorphic thorax phantom, the pathway of a real patient, from imaging to dose delivery. Patient-specific quality assurance (PSQA) measurements were performed with a 2D array, followed by point dose measurements with an ionization chamber in different locations into the phantom: the planning target volume (PTV) and organs at risk (OARs). The combined standard uncertainties associated with point dose measurements were calculated. The results revealed a high quality of IMRT clinical implementation.

Key words: end-to-end test, intensity modulated radiation therapy, patient-specific quality assurance, point dose, uncertainty

1. INTRODUCTION

With the technology advance, the radiotherapy (RT) demand for dosimetric and geometric accuracy has steadily increased. In order to ensure the accuracy of the prescribed dose and to achieve the treatment goal, a Quality Assurance (QA) program is required in all the steps of the RT process, from simulation to treatment administration.

An important aspect in the quality management program is the dosimetry audit. Over the years it was demonstrated that it is a useful tool in ensuring the accuracy and consistency of patient dosimetry and also in maintaining the adequate medical physics practices [1, 2]. Different international organizations recommend that every institution that introduces complex RT techniques in their clinical practice, should participate in an independent dosimetry audit [3, 4].

Nowadays, there are available different levels of audit, from the verification of radiation beam output under reference conditions [5, 6] to overall dosimetry evaluation (end-to-end test) in advanced RT techniques [7-9]. By participating in audit and following the same methodology, the intercomparison processes based on

the obtained results, can help to discover different issues related to some steps of RT chain and also to find out what is achievable with different combination of equipment [10].

In this study, the IMRT treatment chain was verified using the ”end-to-end” approach, i.e. following the pathway of a patient undertaking IMRT treatment in our department, from CT imaging in treatment position, contouring, planning, dose calculation, and dose delivery.

2. MATERIALS AND METHODS

2.1 CIRS THORAX PHANTOM

A CIRS Thorax Phantom 002 LFC (CIRS Inc., Norfolk, Virginia) which represents an average human torso in proportion, density, and 2D structure was used. The phantom body is elliptical (30 cm long × 30 cm wide × 20 cm thick) made of plastic, water, lung, and bone equivalent materials. One half of the phantom is provided with 10 holes which can hold interchangeable inserted rods for dose point measurements with an ionization chamber. The other half of the phantom is divided into 12 sections and can accommodate a film in its coronal plane in order to evaluate 2D dose distributions.

2.2 TREATMENT PLANNING PROCESS

The end-to-end evaluation started with a CT scanning of the phantom with the Siemens Somatom Spirit CT using the local scanning protocol for thorax treatments. The structure delineations (Fig. 1) have been drawn manually in accordance with the guidelines followed by eight RT institutions participating in the International Atomic Energy Agency (IAEA) Coordinated Research Project (CRP) E24017 Program [11]. After that, the contours for each structure, including PTV and five OARs such as spinal cord, esophagus, heart, skin, and lungs were verified.

In this planning process, the dose-volume objectives and constraints, used by the eight RT participating centers, were followed. After the plan was done, the dose-volume histogram (DVH) was calculated for each structure and the results were compared against the provided prescription aims.

The dose calculation was performed by Analytical Anisotropic algorithm based on the 2.5 mm grid size normally used in our center clinical practice and correction for treatment couch.

6 MV photon beams were used to deliver a total prescribed dose of 50.4 Gy in 28 fractions (1.8 Gy dose/fraction) to PTV. The planning goal was that 95% of

the PTV should receive at least 50.4 Gy and the hotspots should be less than 110% of the prescribed dose. The IMRT planning was optimized to meet all the PTV and OAR dose constraints (Table 1).

Table 1

OAR dose constraints used in the IMRT treatment planning process [11]

Critical Structure	Volume (cc)	Maximum volume dose (Gy)	Maximum point dose (Gy)
Spinal Cord	< 1	15.50	17.00
	< 5	14.50	
Esophagus	< 5	44.00	50.50
Heart	< 15	18.00	23.50
Skin	< 10	16.00	24.00
Lungs	500	16.50	50.00

2.3 DOSE DELIVERY AND PHANTOM MEASUREMENTS

CIRS phantom irradiation was performed as if it should be a real patient. The phantom was positioned on the treatment couch and aligned using the treatment room lasers. The IMRT plan was delivered with the UNIQUE™ linear accelerator from Varian Medical System (Palo Alto, CA, USA). The LINAC, which generates high-energy X-rays, is equipped with a multi-leaf collimator (MLC) with 80 leaves and delivers IMRT plans using the sliding window technique.

Taking into account that a correct treatment machine calibration minimizes the misadministration of the prescribed dose, before starting the irradiation, the daily output of the LINAC was verified at point 1 in the phantom (Fig. 2) with the PTW 31010 Semiflex 0.125 cc ionization chamber (PTW Freiburg Inc., Breisgau, Germany). A single field of 6 MV photons with 0° gantry angle, 100 cm source-to-surface distance (SSD), using the nominal dose rate (600 MU/min) and a 10 cm × 10 cm field size with 200 MU (monitor units) was used. The measured dose was determined according to IAEA Technical Reports Series (TRS) No. 398 dosimetry protocol [12] and compared with the Treatment Planning System (TPS) calculated dose under the same conditions as follows:

$$Deviation\ [\ \ ] = 100 \times \left(\frac{D_{calc}}{D_{meas}} - 1 \right) \tag{1}$$

where D_{calc} is the TPS calculated dose and D_{meas} is the measured dose.

After the verification of LINAC beam output, point dose measurements were performed three times in each of the five measurement points (including no. 1 and 2 for dose verification in PTV, no. 5 for the esophagus, no. 6 for the right lung, and no. 10 for the spinal cord) with the Semiflex 0.125 cc ionization chamber and the

average doses were calculated. For all ionization chamber measurements, the absorbed dose to water was determined using the IAEA TRS 398 dosimetry code of practice. The measured doses were compared with the mean TPS calculated doses according to equation (1).

In order to verify the deliverability of the RT plan, patient-specific QA of the IMRT plan was performed using the 2D array, MapCHECK2, and the perpendicular composite (PC) delivery method. 2D dose distribution measurements results were compared to the dose distributions exported from the TPS using gamma analysis [13] with different acceptance criteria, for both global and local gamma analysis (4%/3mm, 3%/3mm, 3%/2mm, and 2%/2mm) and with a 10% low-dose threshold.

3. RESULTS

3.1. TREATMENT PLANING RESULTS

Figure 1 provides an example of the dose distribution calculated with the IMRT technique, in the axial plane of the phantom. In the planning process, seven treatment fields were used at: 5^{o}, 65^{o}, 105^{o}, 225^{o}, 255^{o}, 305^{o}, 345^{o}.

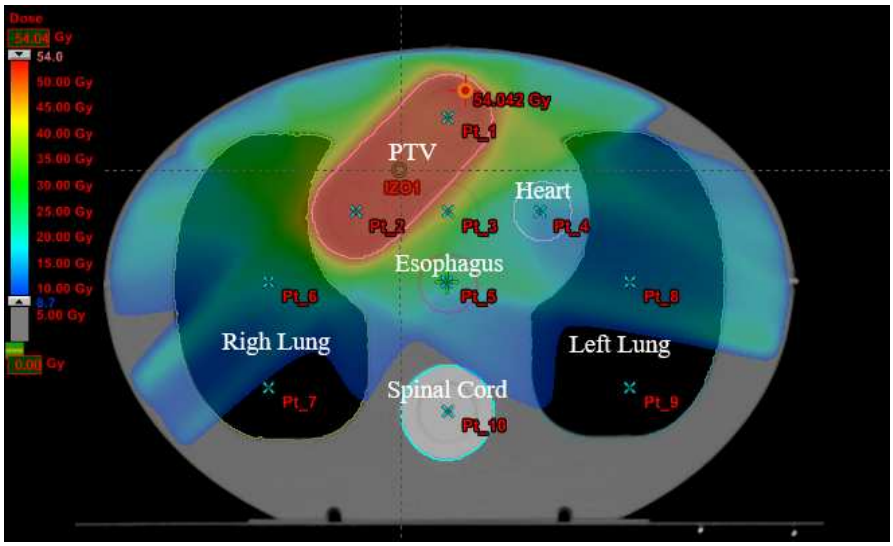

Fig. 1 - Dose color-wash distribution calculated with the IMRT technique in the axial plane of the semi-anthropomorphic thorax phantom

In Table 2, the IMRT plan results are presented. The center basically fulfilled all the dosimetric goals, revealing a high accuracy of the treatment planning model.

Table 2

IMRT treatment planning results

Structure	TPS calculated volume (cc)	Treatment plan objectives	Dose constraints (Gy)	TPS calculated dose (Gy)
Planning	132.75	Maximum point dose	< 55.44	54.04
Target Volume		D95	> 50.40	50.40
Spinal cord	140.91	Maximum point dose	17.00	9.54
		< 1 cc	15.50	7.41
		< 5 cc	14.50	5.73
Esophagus	50.65	Maximum point dose	50.50	32.17
		< 5 cc	44.00	25.38
Heart	73.67	Maximum point dose	23.50	22.55
		< 15 cc	18.00	14.64
Skin	1,346	Maximum point dose	24.00	23.80
		< 10 cc	16.00	11.51
Lungs	4,883	Maximum point dose	50.00	46.62
		500 cc	16.50	11.52

3.2. THE COMBINED STANDARD UNCERTAINTY OF DOSE MEASUREMENT

The dose delivery accuracy has a direct impact on treatment safety and quality. Therefore, the global uncertainty of the process should be reduced as low as possible. For this reason, various uncertainty components were taken into account. They were related to: dosimetry system calibration, ionization chamber reading, correction factors for influence parameters, beam quality correction factor, SSD setting and beam monitor.

The relative standard uncertainties values of ionization chamber and electrometer calibration coefficients were calculated from the values given in the calibration certificates, supplied by the Secondary Standard Dosimetry Laboratory.

As concerns the measurement series, the relative uncertainty of the electrometer reading was calculated and added to the combined standard uncertainty.

The correction factors such as air density, polarity effect, and ion recombination were determined along with their uncertainties. The uncertainty contribution of the air density correction factor was calculated according to IAEA-TECDOC-1585 [14] by taking into consideration the uncertainties of barometer and thermometer resolutions, the uncertainties given in the calibration certificates, and the uncertainties of mean readings. A relative standard uncertainty of 0.09% (k=1) was found.

If during the measurements the relative humidity is close to that given in the calibration certificate, no correction is necessary. According to Das and Zhu [15], in the range of 0%-100% relative humidity, if no correction is made, a maximum error of 0.30% can result. Assuming a rectangular distribution, an uncertainty value of 0.17% (k=1) is obtained.

For the beam quality correction factor, the relative standard uncertainty can reach up to 1.00% (k=1) according to McEwen [16].

The uncertainty contribution regarding SSD setting was calculated considering the maximum deviation of optical distance indicator [17] and assuming a rectangular distribution. A relative uncertainty of 0.12% (k=1) was found.

Knowing that the reading time depends on the selected MUs, the uncertainty contribution related to the beam monitor was calculated based on the display resolution and assuming a rectangular distribution. A relative uncertainty value of 0.14% (k=1) was calculated.

The uncertainty components were summed in quadrature and the combined standard uncertainties for phantom dose measurements were obtained.

3.3. LINAC OUTPUT VERIFICATION

Daily output of the LINAC was verified by comparing the TPS calculated dose with the dose measured at point no.1 into the phantom.

Table 3 shows the percentage of dose difference and the associated standard uncertainty (k=1): -0.42 ± 1.22%.

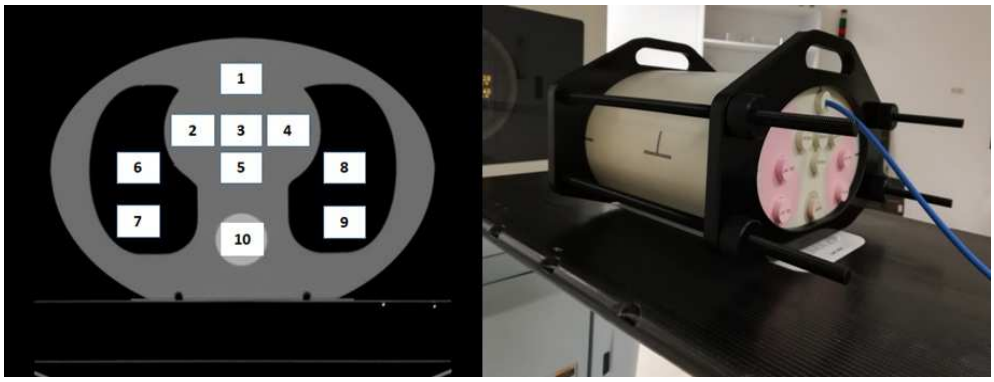

Fig. 2 - LINAC output verification at point no.1 into the CIRS phantom. The TPS calculated dose was compared with the dose measured with the Semiflex 0.125 cc ionization chamber.

Table 3

LINAC output verification. The percentage difference between the TPS calculated and measured dose at point no. 1 into phantom and the associated combined standard uncertainty, u_c (k=1).

TPS calculated dose (Gy)	Measured dose (Gy) ± u_c (%)	Dose difference (Gy) ± u_c (%)
1.897	1.905 ± 1.219	- 0.42 ± 1.22

3.4. POINT DOSE AND PLANAR DOSE DISTRIBUTION MEASUREMENTS

The measured doses at each of the 5 points of interest are shown in Table 4. The percentage differences between the TPS calculated doses and those measured were within ± 3% for PTV, esophagus, right lung and ± 5% for the spinal cord. A combined standard uncertainty (k=1) of 1.22% was obtained for all point dose measurements.
Overall, the results revealed a high accuracy of the TPS dose calculation algorithm.

Table 4

Percentage differences between the TPS calculated and measured doses for PTV and OARs (dose per fraction: 1.8 Gy) and the associated combined standard uncertainties, u_c (k=1).

Structure	TPS calculated volume (cc)	Measured dose (Gy) ± u_c (%)	Dose difference ± u_c (%)
PTV (no. 1)	1.837	1.807 ± 1.219	+1.66 ± 1.22
PTV (no. 2)	1.897	1.854 ± 1.219	+2.32 ± 1.22
Esophagus (no. 5)	0.823	0.841 ± 1.219	-2.14 ± 1.22
Right lung (no. 6)	0.701	0.720 ± 1.219	-2.64 ± 1.22
Spinal cord (no. 10)	0.158	0.166 ± 1.220	-4.82 ± 1.22

Regarding the PSQA measurement, the gamma analysis results are shown in Table 5. For all criteria, the gamma pass rates exceeded 96% which highlighted the LINAC capability to accurately deliver complex IMRT dose distributions.

Table 5

The gamma pass rates for different gamma criteria, for both global and local analysis. The results are given for perpendicular composite (PC) delivery method.

Gamma criterion	Gamma pass rate (%)	
	Global analysis	*Local analysis*
2%2mm	96.7	96.7
3%2mm	100	100
3%3mm	100	100
4%3mm	100	100

4. DISCUSSION

The end-to-end evaluation aimed to verify the IMRT treatment chain, from imaging through treatment planning to the dose delivery using the CIRS Thorax Phantom 002 LFC. After the simulation process and the manual delineation of the structures, it was found that the volumes of structures did not show a degree of variation from those automatically imported by the RT centers participating in the IAEA CRP E24017 Program. Regarding the IMRT planning, the objectives and constraints were basically fulfilled, showing a very good efficiency and robustness of the used TPS version.

According to Kron *et al*. [20] who highlighted the usefulness of checking the treatment machine output along with the end-to-end testing, before starting the dosimetric verification of the IMRT plan, the LINAC beam output was verified in order to minimize misadministration of the prescribed dose. The percentage of dose difference, obtained after performing the verification, was -0.42 ± 1.22%, which represents a result that is well within the tolerance reported in literature [21].

The percentage differences between the TPS calculated doses and those measured in different densities of the phantom were within ± 3% for all structures, excepting the spinal cord for which the -4.82% value was obtained.

Comparing our results with those reported by Tuntipumiamorn et al. [11], where the TPS calculated dose for the spinal cord was underestimated up to 8% and taking into account other multi-institutional IMRT audit results [22-24], one can say that our results satisfy the required accuracy for dose delivery typically quoted as being within ±5% of the prescribed dose [25, 26].

Due to the complexity of the dose distributions which can be achieved with the advanced RT techniques and taking into consideration the information available on the uncertainties in TPS dose calculation algorithm, to report the uncertainties becomes a challenge. In order to achieve a high degree of accuracy, which is required in the modern RT techniques, quantifying and reporting the uncertainties are advised to be done [27]. Given the sources of uncertainty considered in this report, a combined standard uncertainty (k=1) of 1.22% was obtained for the dose measurements. Overall, the results of the present study showed a high accuracy of TPS dose calculation by the used algorithm.

Concerning the patient-specific QA measurement, different gamma criteria were used, for both local and global gamma calculation. Gamma analysis is the most widely used as dose distribution comparison method. Also, the acceptability criterion of 3%/3mm (global normalization in absolute dose) for a pass rate greater than 95% is the most adopted in the majority of RT centers. In order to consider the treatment plan clinically acceptable, AAPM TG 218 [28] task group recommends using the true composite delivery method based on a 3D measurement with a high

spatial resolution detector and having a pass rate greater than 95% for 3%2mm criterion and global normalization in absolute dose. Other publications [29-31] recommend to use a tighter criterion such as 2%2mm which can help to detect MLC positional errors.

The gamma pass rates obtained in this report ranged from 96.7% for 2%2mm (local analysis) to 100% for 4%3mm (global analysis). Given the irradiation conditions presented in this study for the 2D dose measurements, the gamma analysis results are in agreement with the average pass rates of the eight RT centers participating in CRP E24017 Program. As it can be seen, the gamma pass rates for 3%2mm and 3%3mm criteria were 100%, showing a very good capability of the treatment machine to deliver IMRT dose distributions.

The IMRT patient-specific QA results performed with the Unique Varian machine were in good agreement with those reported by Servavalli *et al*. [32] which used a set of predefined treatment plans to audit local methods for QA in RT.

5. CONCLUSIONS

The end-to-end testing with the CIRS Thorax Phantom, 002LFC, has helped to verify different steps of the RT treatment chain and to evaluate the physical aspects of the thorax cancer IMRT treatments.

The quality of the IMRT treatment was checked from a physics perspective by comparing the calculated and measured doses in different density points into the phantom. This also helped to verify how the heterogeneities are accounted in TPS calculations.

Dose measurements results showed that an accurate treatment delivery, within the admitted tolerance, was achieved.

Overall, the planning and measurements results have confirmed a safe use of the IMRT technique for thorax treatments in the radiotherapy department and revealed a high quality of IMRT clinical implementation.

REFERENCES

1. D. J. Eaton, S. Bolton, R. A. S. Thomas, C. H. Clark, *J. Med. Phys.* **40**(4), 183–189 (2015).
2. C. H. Clark, N. Jornet, L. P. Muren, *Phys. Imaging Radiat. Oncol.* **5**, 85–87 (2018).
3. J. Izewska, W. Lechner, P. Wesolowska, *Phys. Imag. Radiat. Oncol.* **5**, 1–4 (2018).
4. International Atomic Energy Agency (IAEA), *SSDL Newsletter No. 70* (2019).
5. J. Izewska, P. Andreo, *Radiother. Oncol.* **54**(1), 65–72 (2000).
6. M. A. Bolt, C. H. Clark, T. Chen, A. Nisbet, *Phys. Imag. Radiat. Oncol.* **4**, 39–43 (2017).
7. A. Molineu, N. Hernandez, T. Nguyen, G. Ibbott, D. Followill, *Med. Phys.* **40**(2), 022101 (2013).

8. H. Schiefer, A. Fogliata, G. Nicolini, L. Cozzi, W. W. Seelentag, E. Born, F. Hasenbalg, J. Roth, B. Schnekenburger, K. Munch-Berndl, V. Vallet, M. Pachoud, B. Reiner, G. Dipasquale, B. Krusche, M. K. Fix, *Med. Phys.* **37**(8), 4424-4431 (2010).
9. P. Kazantsev, W. Lechner, E. Gershkevitsh, C. H. Clark, D. Venencia, J. Van Dyk, P. Wesolowska, P. Hernandez, N. Jornet, M. Tomsej, T. Bokulic, J. Izewska, *Acta Oncolog.* **59**(2), 144-148 (2020).
10. D. S. Followill, S. F. Kry, L. Qin, J. Leif, A. Molineu, P. Alvarez, J. F. Aguirre, G. S. Ibbott, *J. Appl. Clin. Med. Phys*. **13**(5), 282-289 (2012).
11. L. Tuntipumiamorn, P. Tangboonduangjit, T. Sanghangthum, R. Rangseevijitprapa, C. Khamfongkhruea, T. Niyomthai, B. Vuttiprasertpong, S. Supanant, N. Chatchaipaiboon, P. Iampongpaiboon, P. Nakkrasae, T. Jaikuna, *Rep. Pract. Oncol. Radiother*. **24**(1), 124-132 (2019).
12. International Atomic Energy Agency (IAEA), *"Absorbed Dose Determination in External Beam Radiotherapy: An International Code of Practice for Dosimetry based on Standards of Absorbed Dose to Water", IAEA Technical Reports Series No. 398*, IAEA, Vienna, 2000.
13. D. A. Low, W. B. Harms, S. Mutic, J. A. Purdy, *Med. Phys.* **25**(5), 656-661 (1998).
14. International Atomic Energy Agency (IAEA), *"Measurement Uncertainty, A Practical Guide for Secondary Standards Dosimetry Laboratories", IAEA Technical Documents No. 1585*, IAEA, Vienna, 2008.
15. I. J. Das, T. C. Zhu, *Med. Phys.* **31**(3), 573-578 (2004).
16. M. R. McEwen, *Med. Phys*. **37**(5), 2179-2193 (2010).
17. E. E. Klein, J. Hanley, J. Bayouth, F. F. Yin, W. Simon, S. Dresser, C. Serago, F. Aguirre, L. Ma, B. Arjomandy, C. Liu, C. Sandin, T. Holmes, *Med. Phys.* **36**(9), 4197-4212 (2009).
18. C. J. Hourdakis, K. Zourari, Z. Thrapsanioti, A. Boziari, *Dosimetry Audits in Greek Radiotherapy Centers: EEAE's 15 years' experience and contribution – Summary Report*, Greek Atomic Energy Commission (EEAE), Athens, 2018.
19. A. Ahnesjö, M. M. Aspradakis, *Phys. Med. Biol.* **44**(11), R99-155 (1999).
20. T. Kron, C. Hamilton, M. Roff, J. Denham, *Int. J. Radiat. Oncol. Biol. Phys*. **52**(2), 566–579 (2002).
21. International Atomic Energy Agency (IAEA), Dosimetry audit networks (DAN) database: on-site 'end-to-end' dosimetry audits, 2019. Available from: https://dosimetry-audit-networks.iaea.org/Home/EndToEndAudits.
22. T. Santos, M. do Carmo Lopez, E. Gershkevitsh, F. Vinagre, D. Faria, L. Carita, M. Pontes, S. Vieira, E. Poli, S. Faustino, F. Ribeiro, M. Trindade, F. Ponte, C. Marcelino, C. Batista, S. Oliveira, R. Figueira, J. Lencart, E. Gallego Diaz, K. Jacob, S. Bras, R. Pirraco, J. Izewska, *Phys. Med*. **65**, 128-136 (2019).
23. P. Wesolowska, D. Georg, W. Lechner, P. Kazantsev, T. Bokulic, A. Carlsson Tedgren, E. Adolfsson, A. M. Campos, V. G. L. Alves, L. Suming, W. Hao, D. Ekendahl, I. Koniarova, W. Bulski, J. L. A. Samper, S. P. Vinatha, P. Rakshit, S. Siri, M. Tomsejm, M. Tenhunen, J. Povall, S. F. Kry, D. S. Followill, D. S. Thaites, J. Izewska, *Acta Oncol*. **58**(12), 1731-1739 (2019).
24. G. Budgell, J. Berresford, M. Trainer, E. Bradshaw, P. Sharpe, P. Williams, *Radiother. Oncol.* **99**(2), 246–252 (2011).
25. D. Thwaites, *J. Phys. Conf. Ser*. **444**, 012006 (2013).
26. B. J. Mijnheer, J. J. Battermann, A. Wambersie, *Radiother. Oncol*. **8**(3**)**, 237-252 (1987).
27. D. van der Merwe, J. van Dyk, B. Healy, E. Zubizarreta, J. Izewska, B. Mijnheer, A. Meghzifene, *Acta Oncol.* **56**(1), 1-6 (2017).
28. M. Miften, A. Olch, D. Mihailidis, *Med. Phys*. **45**(4), e53-e83 (2018).

29. J. M. Park, J. Kim, S. Y. Park, D. H. Oh, S. T. Kim, *Radiat. Oncol*. **13**(1), 175 (2018).
30. L. Yu, T. L. S. Tang, N. Cassim, A. Livingstone, D. Cassidy, T. Kairn, S. B. Crowe, *J. Appl. Clin. Med. Phys*. **20**(11), 189-198 (2019).
31. B. E. Nelms, M. F. Chan, G. Jarry, M. Lemire, J. Lowden, C. Hampton, V. Feygelman, *Med. Phys*. **40**(11), 111722 (2013).
32. E. Seravalli, A. C. Houweling, L. V. Battum, T. A. Raaben, M. Kuik, J. A. Pooter, M. P. R. Van Gellekom, J. Kaas, W. Vries, E. L., J. B. van de Kamer, *Phys. Imag. Radiat. Oncol*. **5**, 19-25 (2018).